

Accelerating Graph Neural Networks on Real Processing-In-Memory Systems

Christina Giannoula^{*†}, Peiming Yang^{*}, Ivan Fernandez Vega^{§†}, Jiacheng Yang^{*}, Yu Xin Li^{*},
Juan Gomez Luna^{¶†}, Mohammad Sadrosadati[†], Onur Mutlu^{†‡}, Gennady Pekhimenko^{*||}

^{*}University of Toronto

[†]ETH Zürich

[§]Barcelona Supercomputing Center

[¶]NVIDIA

[‡]Stanford

^{||}CentML

Abstract—Graph Neural Networks (GNNs) are emerging ML models to analyze graph-structure data. Graph Neural Network (GNN) execution involves both compute-intensive and memory-intensive kernels, the latter dominates the total time, being significantly bottlenecked by data movement between memory and processors. Processing-In-Memory (PIM) systems can alleviate this data movement bottleneck by placing simple processors near or inside to memory arrays. In this work, we introduce PyGim, an efficient ML framework that accelerates GNNs on real PIM systems. We propose intelligent parallelization techniques for memory-intensive kernels of GNNs tailored for real PIM systems, and develop handy Python API for them. We provide hybrid GNN execution, in which the compute-intensive and memory-intensive kernels are executed in processor-centric and memory-centric computing systems, respectively, to match their algorithmic nature. We extensively evaluate PyGim on a real-world PIM system with 1992 PIM cores using emerging GNN models, and demonstrate that it outperforms its state-of-the-art CPU counterpart on Intel Xeon by on average 3.04 \times , and achieves higher resource utilization than CPU and GPU systems. Our work provides useful recommendations for software, system and hardware designers. PyGim will be open-sourced to enable the widespread use of PIM systems in GNNs.

I. INTRODUCTION

Graph Neural Networks (GNNs) have emerged as state-of-the-art Machine Learning (ML) models that provide high accuracy in node classification and link prediction [50], [54] thanks to their ability to depict dependent relationships in graph-structure data. Thus, they have been adopted to real-world applications, including point-cloud analysis [47], recommendation systems [57], social network analysis [14], and drug discovery [51]. GNNs comprise a few layers, and each layer consists of two steps: the *aggregation* and *combination* step. The former aggregates the input feature vectors of the neighboring vertices for each vertex in the graph via a permutation-invariant operator (e.g., average). The latter processes the aggregated vectors of all vertices through a small neural network (e.g., a multilayer perceptron) to produce the output feature vectors that are fed as input feature vectors to the next subsequent layer.

In this study, we profile the GNN execution in commodity ML systems, and find that combination is a compute intensity step, while aggregation exhibits high memory intensity. The key operators of combination are dense matrix matrix multiplications (GEMMs), which are computationally expensive and fit well to be executed in processor-centric systems (CPUs

or GPUs). However, aggregation is significantly bottlenecked by data movement between memory and processors in such systems. This is because this step processes the input real graph, that is typically very sparse [17], [40], and degenerates to a Sparse Matrix Matrix Multiplication (**SpMM**) kernel, that has low arithmetic intensity, and is memory-bandwidth-bound in CPUs/GPUs for the majority of real graphs.

One way to alleviate the data movement cost is Processing-In-Memory (PIM) [12], [33], [41] computing paradigm. PIM moves computation close to data by equipping memory chips with processing capabilities. To provide significantly higher memory bandwidth for the in-memory processors than standard DRAM modules, *near-bank* PIM designs have been recently manufactured [12]. Near-bank PIM systems tightly couple a PIM core with one (or a few) DRAM bank, exploiting bank-level parallelism to expose high on-chip memory bandwidth of standard DRAM to processors. The UPMEM PIM architecture [12] is the first PIM system to become commercially available.

Our **goal** is to quantify the potential of real PIM architectures in GNNs, and propose intelligent techniques to accelerate the GNN execution in PIM systems. We propose **PyGim**, an easy-to-use ML framework that efficiently executes GNNs in PIM systems, and we make four key innovations.

First, we employ a **Combination of Accelerators (CoA)** scheme, in which heterogeneous kernels run to different accelerators: the processor-centric CPU or GPU system (named **Host**) executes the compute-intensive combination of GNNs, and the memory-centric PIM system executes the memory-intensive aggregation. Although a few works [55], [61], [65] provide hybrid CPU-PIM designs for GNNs, they propose new *hardware* architectures, use software emulators for their evaluations, and design *near-rank* PIM systems (rank-level parallelism for in-memory cores). Instead, PyGim proposes system- and software-level optimization techniques, evaluates GNNs on *real* commercially available PIM systems, and targets *near-bank* PIM designs, that provide higher memory bandwidth than near-rank designs [33], and are already available in the market. To our knowledge, PyGim is the first work to provide *real* Host-PIM execution in GNNs.

Second, we propose **Hybrid Parallelism (HP)** for GNN aggregation: PyGim enables three levels of parallelism on the hardware PIM side, and at each level provides a different

parallelization technique on the software side. 1) We group the available PIM cores of the system in clusters, and design **edge- and feature-level parallelism across PIM clusters**. 2) We enable **vertex- or edge-level parallelism across cores within PIM cluster**. 3) We also employ either **vertex- or edge-level parallelism across threads within a PIM core**. HP strives a balance between computation and data transfer costs, since the first parallelization scheme reduces data transfer overheads to/from PIM memory modules, while the last two schemes provide high compute balance across low-power PIM cores and across threads within a PIM core. Our work is the first to efficiently execute GNN aggregation on real near-bank PIM systems.

Third, we develop a PIM backend for our optimized GNN aggregation, and expose it with a handy Python API, so that programmers can easily use it. We integrate our API with PyTorch [43] (it can be integrated to other frameworks) to support both CPU-PIM and GPU-PIM execution for GNNs. To our knowledge, PyGim is the first easy-to-use ML framework that supports efficient GNN execution tailored for PIM systems, and will be open-source available to enable the use of PIM systems in ML inference.

Fourth, we comprehensively characterize GNN inference on the UPMEM PIM system, the first real-world PIM architecture. We evaluate our techniques in terms of scalability, data transfer costs, aggregation kernel and end-to-end performance using various real-world graphs and GNN models. We demonstrate that PyGim outperforms a state-of-the-art CPU baseline by on average $3.07\times$ and $3.04\times$ in aggregation and end-to-end performance, respectively, and provides higher resource utilization than CPU and GPU systems. Our extensive evaluations provide recommendations to improve multiple aspects of future PIM hardware and software.

II. BACKGROUND & MOTIVATION

A. Graph Neural Networks (GNNs)

GNNs are emerging ML models to analyze graph-structured data (knowledge graphs, social and road networks). A GNN model has a few layers. Each layer takes as input (i) the graph $G = (V, E)$, where V and E represent the graph's vertices and edges (connections between vertices), which is stored as a matrix, henceforth referred to as **adjacency matrix** A , and (ii) the *feature* matrix F , that has one feature vector per vertex in the graph, each vector encodes the vertex's characteristics. Real-world graphs are typically sparse (less than 0.1%) [17], [61]. They have relatively few connections between vertices compared to the total number of possible connections. Thus, the adjacency matrix is stored in memory with a compressed format, e.g., Compress Sparse Row (CSR) [4]. Instead, the feature matrix is dense with size $N \times K$, where N is the number of vertices and K is the number of features per vertex (henceforth referred to as **hidden size**).

Fig. 1 shows the GNN layer execution that has two steps: the *aggregation* and *combination*. In aggregation, each vertex gathers the feature vectors of its neighbors, and produces an aggregated vector through an operator (e.g., average). In

combination, the aggregated vectors of all vertices are processed through a small neural network, that typically has dense operators (e.g., GEMMs) and finishes with an activation. The output feature vectors of all vertices serve as an input feature matrix of the next layer in GNN model.

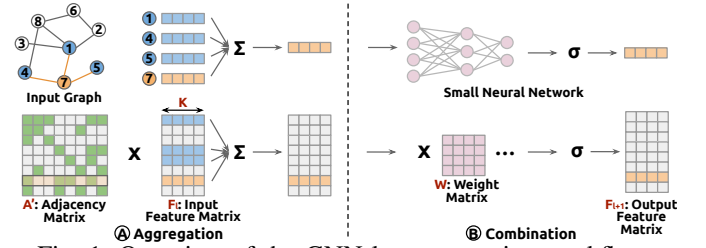


Fig. 1: Overview of the GNN layer execution workflow.

The operators of aggregation and combination slightly vary across GNN models. For example, GCN [29] uses *weighted sum* function for aggregation, while GIN [58] uses *sum* function. Similarly, GIN uses an MLP for combination, while SAGE [22] uses a fully-connected operator. Assuming that A' is a normalized adjacency matrix based on the aggregation operator of each particular model, F^l is the input feature matrix of a layer l with hidden size K , and W_i^l matrices are weight matrices used in the small neural network of combination, the GNN computation can be expressed as:

$$F^{l+1} = \sigma(\sigma((A' * F^l) * W_1^l) \dots * W_w^l)$$

F^{l+1} will be the input feature matrix of the next layer. The aggregation step corresponds to the computation $A' * F^l$, which is a Sparse Matrix Matrix Multiplication (SpMM).

B. GNN Execution in Commodity Systems

Recent works [55], [61], [65] show that GNN aggregation takes the largest portion of the execution time, being more than 50%, because it is bottlenecked by data movement in CPUs and GPUs. We evaluate GNNs in a high-end GPU (See Table III) and observe that aggregation takes more than 91% of total time. Fig. 2 shows the roofline model, when executing an aggregation and combination in RTX 3090. Even with a state-of-the-art GPU with more than 900GB/s available bandwidth, combination is a compute-intensive kernel, while aggregation is in the memory-bound area, and is significantly limited by memory bandwidth, thus being potential suitable for PIM.

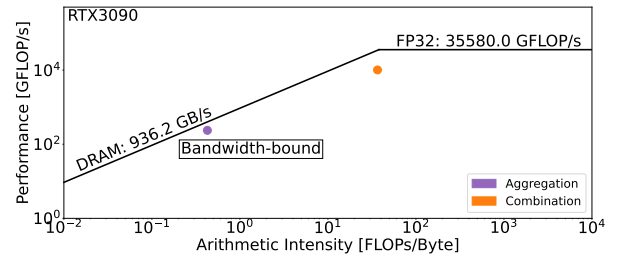


Fig. 2: Roofline model in the NVIDIA RTX 3090 GPU for aggregation and combination execution.

C. Near-Bank Processing-In-Memory (PIM) Systems

PIM computing paradigm [41] enables memory-centric computing systems: processing units (general-purpose cores or specialized accelerators) are placed near or inside memory arrays. PIM is a feasible solution to alleviate the data movement bottleneck of processor-centric systems. To provide high memory bandwidth, several manufacturers [12], [33], [34] explore near-bank PIM designs, which tightly couple a PIM core with one (or a few) DRAM bank, exploiting bank-level parallelism. Near-bank PIM systems enable high levels of parallelism, since they can support *thousands* of PIM cores.

Near-bank PIM systems are a reality, with the commercialization of the UPMEM PIM [12], and the announcement of HBM-PIM [34] and AiM [33] (the last two prototyped and evaluated in real systems). UPMEM places a general-purpose core near each memory bank of a DDR4 DRAM chip. HBM-PIM has a SIMD unit with 16-bit floating point support between every two banks in memory layers of HBM stack. AiM is a GDDR6-based PIM architecture with near-bank cores that support multiply-and-accumulate and activation operations.

These real-world PIM systems have some important common characteristics, shown in Fig. 3. First, there is a Host processor (CPU or GPU) typically with a deep cache hierarchy, which is connected to standard main memory and PIM-enabled memory. Second, the PIM-enabled memory module has one (or a few) memory devices (rank of 2D DRAM or stacked layer of 3D-stacked DRAM). Each PIM device contains multiple processing elements (PIM cores), that have access to memory banks with higher bandwidth and lower latency than the Host cores. Third, the PIM cores (general-purpose cores, SIMD units, or specialized processors) run at only a few hundred megahertz, and have relatively small (or no) scratchpad or cache memory. Fourth, PIM cores may not be able to directly communicate with each other (UPMEM, HBM-PIM or AiM in different chips), and communication between them happens via the Host.

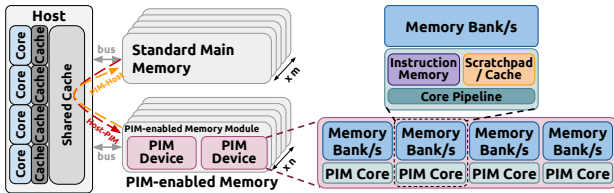


Fig. 3: High-level view of a real near-bank PIM system. Host has access to m standard and n PIM-enabled memory modules.

In our evaluation, we use UPMEM PIM [12], the first PIM system that has been commercialized in real hardware. UPMEM PIM uses 2D DRAM arrays and combines them with general-purpose cores, called *DPUs*, on the same chip. Each PIM-enabled module has two ranks (devices), each rank has 8 chips, and each chip has 8 DPUs. Each DPU is tightly coupled to a DRAM bank, has a 14-stage pipeline and supports multiple threads (up to 24), called *tasklets*.

DPUs have a 32-bit RISC-style general-purpose instruction set, and natively support in hardware 32-bit integer addition/-

subtraction and 8-bit/16-bit multiplication, but more complex operations (e.g., 32-bit integer multiplication/division) and floating-point operations are software emulated [21]. Each DPU has access to its own (1) 64MB DRAM bank, called MRAM, (2) 24KB instruction memory, and (3) 64KB scratchpad memory, called WRAM. The Host CPU can access the MRAM banks to copy input data (from main memory to MRAM, i.e., CPU-DPU) and retrieve results (from MRAM to main memory, i.e., DPU-CPU). The CPU-DPU/DPU-CPU transfers can be performed in parallel across multiple MRAM banks, if the size of data transferred from/to all MRAM banks is the same. Since there is no direct communication channel between DPUs, inter-DPU communication takes place via the Host.

In our paper, we use a generic terminology, since our optimization strategies can generally apply to near-bank PIM systems, like the generic one shown in Fig. 3, and not exclusively to the UPMEM PIM. Thus, we use the terms PIM device, PIM core, PIM thread, DRAM bank, scratchpad, and Host-PIM/PIM-Host data transfer, corresponding to PIM rank, DPU, tasklet, MRAM bank, WRAM, and CPU-DPU/DPU-CPU data transfer in UPMEM's terminology.

III. PYGIM : DESIGN AND OPTIMIZATIONS

PyGim is a novel ML framework that accelerates GNNs on real PIM systems. PyGim improves system performance by effectively executing compute-bound and memory-bound kernels on processor-centric and memory-centric hardware, respectively (Section III-A), and providing highly efficient parallelization strategies in GNN aggregation tailored for real PIM systems (Section III-B), and it enables high programming ease via a high-level ML-friendly interface (Section III-C).

A. Combination of Accelerators (CoA)

GNN execution alternates between sparse and dense operations: the aggregation step degenerates to an SpMM, which is bottlenecked by memory bandwidth in processor-centric systems (Fig. 2), while the combination step mainly comprises compute-heavy kernels, e.g., GEMMs. We propose a *Combination of Accelerators (CoA)* scheme that efficiently maps and executes each step to the best-fit underlying hardware. For *each* GNN layer, PyGim executes the SpMM kernel of aggregation on PIM cores to leverage immense memory bandwidth available on PIM system, and the compute-heavy kernels of combination on Host (CPU or GPU) to exploit large processing capabilities available on processor-centric systems. Since aggregation and combination steps are repeated the one after the other in multiple GNN layers, the **key challenge** is how to minimize the overheads of passing the output of the one step as input to the next step. We discuss how we address it in the next subsection. Note that while PIM cores are executing aggregation, Host cores are idle, until the dependent computation is finished, and vice versa. We leave for future work the extension of PyGim to offload part of aggregation and combination computation on Host and PIM cores, respectively, to minimize idleness.

B. Hybrid Parallelism (HP)

Fig. 4 shows the GNN aggregation step execution on a real PIM system that can be broken down in four steps: (1) the time transfer the input feature matrix from Host into DRAM banks of PIM-enabled memory (**Host-PIM**), (2) the time to execute computational kernel on PIM cores (**Kernel**), (3) the time to retrieve from DRAM banks of PIM-enabled memory to the Host the results for the output (**PIM-Host**), and (4) the time to merge partial results and assemble the final output feature matrix on the Host (**Merge**). In our study, we omit the time to load the adjacency matrix into PIM-enabled memory. This is because the adjacency matrix is *reused* across all layers, and needs to be loaded only *once* into PIM-enabled memory, i.e., when reading the graph file from the disk and loading it to DRAM (pre-processing step).

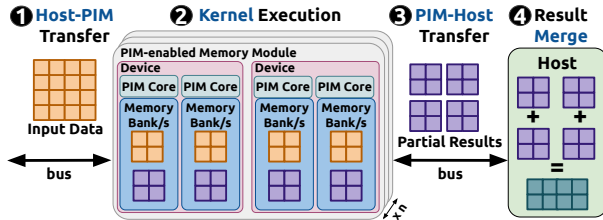


Fig. 4: Execution of the aggregation step on a real PIM system.

Naive strategies to execute PIM aggregation would be to equally parallelize (i) the vertices or (ii) edges across PIM cores. These would cause excessive data transfer overheads, thus do not address the key challenge mentioned above. In the (i) case, the large feature matrix needs to be copied and replicated at *each* PIM core of the system, thus incurring high Host-PIM overheads. In the (ii) case, each PIM core would create a large partial result array that needs to be retrieved and merged by Host, thus causing high PIM-Host overheads. Moreover, a parallelization scheme that assigns one column (feature) of the feature matrix to be processed at each PIM core would incur high computation costs, since each core processes *all* graph’s vertices and edges causing high kernel time, or would leave many PIM cores idle, since GNN layers may have a smaller hidden size (e.g., 128) than the available PIM cores of the system (thousands of cores).

To efficiently execute PIM aggregation, we propose *Hybrid Parallelism* (HP). PyGim supports three levels of parallelism, each level implements a different strategy, shown in Fig. 5. The key idea is that the first level parallelization strategies reduce data transfer overheads (Host-PIM and PIM-Host), thus addressing the aforementioned key challenge, while the second and third level parallelization strategies reduce computation overheads (kernel time). This way PyGim’s HP provides the sweet-spot and strives a balance between computation and data transfer costs.

Across PIM Clusters. We group the available PIM cores into clusters, named **PIM clusters**, and execute a part of the SpMM aggregation at each cluster. A PIM device can contain multiple PIM clusters, while all cores of the same cluster belong to the same PIM device (grouping cores located to different PIM

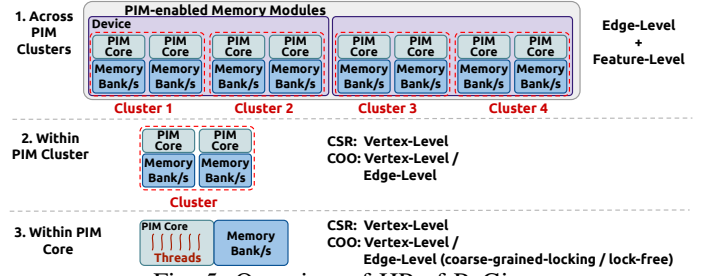


Fig. 5: Overview of HP of PyGim.

devices is inefficient, since it would need multiple *separate* Host-PIM / PIM-Host transfers for the *same* cluster, causing high transfer and launch overheads).

We parallelize SpMM across PIM clusters via a hybrid **edge-level** and **feature-level** approach, shown in Fig. 6. Each cluster processes a subset of the graph’s edges and a subset of the vertices’ features to minimize Host-PIM/PIM-Host transfer costs. We create vertical partitions (edge-level parallelism) on the adjacency sparse matrix (henceforth refer to as **sparse partitions**), each partition is assigned to multiple PIM clusters. In Fig. 6, there are 2 sparse partitions, and clusters 1, 2 process the orange edges, while clusters 3, 4 process the blue edges of the graph. To minimize the amount of partial results produced for the final output matrix due to edge-level parallelism, we combine it with feature-level parallelism, i.e., creating vertical partitions on the feature dense matrix (henceforth refer to as **dense partitions**). Edge-level and feature-level parallelism split the feature matrix in 2D tiles, the number of which is equal to the number of PIM clusters used. Multiple clusters process in parallel the 2D tiles of the feature matrix, thus executing a part of the SpMM. Fig. 6 has four feature matrix tiles.

Assuming a graph with N vertices, hidden size K and R PIM clusters, when creating L equal partitions on the feature matrix ($L < R$), each PIM cluster processes a feature matrix tile of size $(N/(R/L)) \times (K/L)$ (Host-PIM transfer), and produces a partial output matrix of size $N \times (K/L)$ (PIM-Host transfer). Note that although in the example of Fig. 6 the adjacency and feature matrices are equally partitioned across clusters, i.e., the sparse and dense partitions have the same column width, PyGim is configurable and supports variable-sized vertical partitions on the adjacency and feature matrices. However, with variable-sized partitions, PIM clusters process variable-sized 2D feature tiles and produce variable-sized partial output results. Our preliminary evaluations showed that this approach incurs high load imbalance in Host-PIM/PIM-Host transfers, causing high overheads. Thus, in our evaluations we present equal-sized partitions.

Within PIM Cluster. PyGim encodes the adjacency matrix with CSR [4], [46] or COO [46], [49] format, which are the state-of-the-art compressed storage formats for sparse matrices [25], [32], [40], [45]. We parallelize the smaller SpMMs across PIM cores within the same cluster, by enabling *vertex-level* parallelism, if the adjacency matrix is stored in CSR, and either *vertex-level* parallelism or *edge-level*

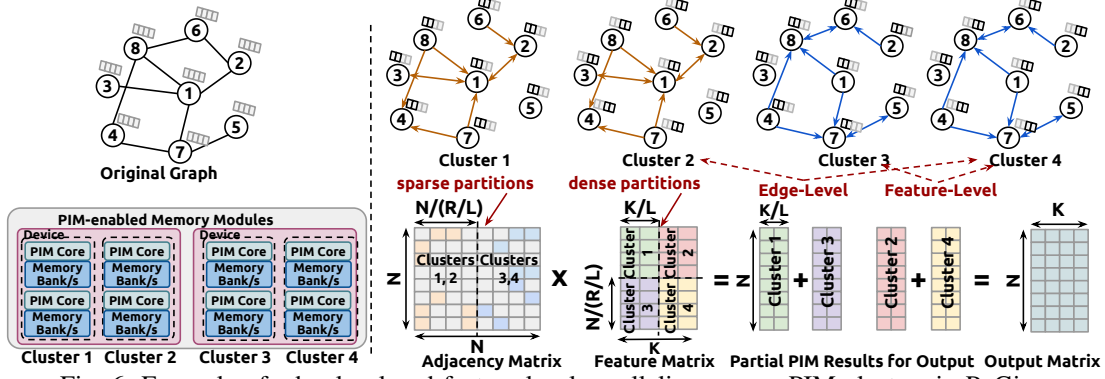


Fig. 6: Example of edge-level and feature-level parallelism across PIM clusters in PyGim.

parallelism, if it is stored in COO. This way we provide compute balance across cores of the same cluster, minimizing the kernel time. The corresponding 2D feature matrix tile is replicated at each core of the same PIM cluster. Fig. 7 presents an example of parallelization across multiple cores of the *same* cluster with CSR and COO formats.

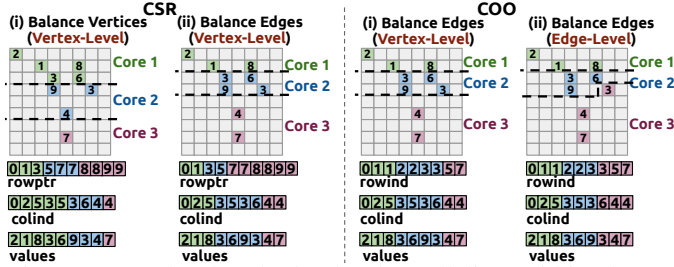


Fig. 7: Vertex-level and edge-level parallelism within cluster.

CSR format (Fig. 7 left) sequentially stores the edges (non-zero elements) in a vertex-wise (row) order. A column index array (*colind[]*) and a value array (*values[]*) store the column index and value of each non-zero element, respectively. An array, named *rowptr[]*, stores the location of the first non-zero element of each row within the *values[]* array. The adjacent pair *rowptr[i, i+1]* stores the number of the non-zero elements of the *i*-th row. Since in CSR the adjacency matrix is stored in vertex-wise order, we perform *vertex-level* parallelism across PIM cores of the same cluster: each core processes a subset of the vertices, i.e., consecutive rows in the adjacency matrix. We provide two load-balancing schemes: (i) equally balancing the number of vertices (rows) across PIM cores (Fig. 7 left i), and (ii) equally balancing the number of edges (non-zero elements) across PIM cores at vertex (row) granularity (Fig. 7 left ii).

COO format (Fig. 7 right) stores metadata of edges (non-zero elements) in three arrays: the row index (*rowind[]*), column index (*colind[]*) and value (*values[]*) arrays store the row index, column index and value of each non-zero element, respectively. Since in COO the adjacency matrix is stored in *non-zero-element-wise order* (edge-wise order), we enable either *vertex-level* parallelism, i.e., each PIM core of the cluster processes a subset of the vertices, or *edge-level* parallelism, i.e., each PIM core processes a subset of the edges. We provide two schemes: (i) equally balancing the number of edges (non-zero elements)

across cores at a vertex (row) granularity (Fig. 7 right i), and (ii) equally balancing the number of edges (non-zero elements) across cores by enabling splitting a vertex (row) across two (or more) neighboring cores to provide a near-perfect edge-level balance (Fig. 7 right ii). In the latter case, when a vertex (row) is split between neighboring PIM cores, the cores produce partial results for the same row of the output matrix, which are transferred and merged by Host cores.

Within PIM Core. We follow similar parallelization approach across threads within a PIM core with that enabled across PIM cores of the same cluster (Fig. 7). We enable high compute balance across threads of the same core to further minimize the kernel time. In CSR, we perform *vertex-level* parallelism by either (i) equally balancing the number of vertices (rows) across threads of a core, or (ii) equally balancing the number of edges (non-zero elements) at a vertex (row) granularity across threads. In COO, we either (i) equally balance the number of edges (non-zero elements) at a vertex (row) granularity across threads of a core (vertex-level parallelism), or (ii) equally balance the number of edges (non-zero elements) across threads, enabling splitting a vertex (row) across two (or more) PIM threads (edge-level parallelism). In the latter, when a vertex (row) is split across two (or more) PIM threads, PIM threads perform write accesses to the *same* elements of the output matrix, thus synchronization among threads is necessary. PyGim provides two synchronization schemes:

- **coarse-grained locking:** one global mutex (lock) protects all the elements of the output matrix.
- **lock-free:** race conditions might arise in only a few elements, when a vertex (row) is split across two (or more) threads, i.e., the number of competing elements are proportional to the number of threads of a core, which are a few. Thus, threads temporarily store partial results for these few elements in the scratchpad memory, and then one single thread merges the partial results, and writes the final result to the DRAM bank/s with no synchronization.

Kernel Implementation. We describe how threads access the data involved in SpMM. There are three types of data structures: (i) the arrays that store the non-zero elements of the adjacency matrix, i.e., their values (*values[]*) and their positions *rowptr[]*, *colind[]* for CSR, and *rowind[]*, *colind[]* for COO, (ii) the array that stores the elements of the feature matrix, and (iii) the array

that stores the partial results for the output matrix. First, SpMM performs streaming memory accesses to the arrays that store the non-zero elements. To exploit immense bandwidth, each thread reads the non-zero elements (their values and positions) by fetching large chunks of bytes in a coarse-grained manner from DRAM bank to scratchpad. Then, it accesses elements through scratchpad in a fine-grained manner. In the UPMEM PIM system, we fetch large chunks of 128-bytes/256-bytes, as suggested by prior work [20]. Second, SpMM processes the feature matrix elements at a row granularity, as a chunk of hidden size elements in the tile assigned to the PIM core, e.g., a chunk of K/L elements in Fig. 6. To exploit spatial locality, each thread reads the feature matrix elements by fetching chunks of tile hidden size \times data type bytes from DRAM bank to scratchpad, and performs multiply-and-add. Third, threads temporarily store partial results for the elements of the same output matrix row in scratchpad, until all non-zero elements of the same row of the adjacency matrix are processed, in order to exploit temporal locality for multiple updates on the *same* output matrix elements. Then, the produced results are written from scratchpad to DRAM bank/s at coarse granularity as a chunks of tile hidden size \times data type bytes.

Merge Step. PyGim merges partial results created across PIM clusters and across cores within PIM cluster (merge step) by executing a parallel reduction operation on Host. In our CPU-PIM system, we use the OpenMP API [8] and perform a 2D block reduction for each partial result block to the final output matrix.

C. PyGim API and Integration

Combination comprises a small neural network, thus PyGim leverages existing optimized ML kernels from Pytorch to execute the corresponding ML operators of GNN combination on Host cores. We integrate PIM aggregation with PyTorch, as we explain in the next paragraph. Note that although we only have access to a CPU-PIM system for our evaluations, PyGim also supports GPU-PIM GNN executions by leveraging PyTorch’s supported backends (CPU and GPU). This way PyGim can be executed to recently commercialized CPU-PIM systems, as well as GPU-PIM systems that are expected to be available in the market in the near future.

To interact with PIM devices (e.g., Host-PIM/ PIM-Host transfers) in aggregation, Host code also needs to be implemented. The Host code implements the parallelization approaches proposed in Section III-B and the corresponding data partitioning schemes, and it is developed in C language, in order to be effectively used and integrated to many real PIM systems. The kernel code that PIM cores are running is implemented using the UPMEM PIM interface, since this is the only commercially-available real PIM system. However, this interface is also written using C language, thus it can be easily ported in other PIM systems with similar interfaces with UPMEM. We create a PIM backend for PIM aggregation and expose this software runtime as a handy Python API so that users can easily use it via a high-level programming interface. We combine our Python-like API with PyTorch [43] to enable efficient CoA execution. Alg. 8 presents an example of the

```

1 import torch, pygim as gyn
2 class GCNConv(torch.nn.Module):
3     def __init__(self, hidden_size):
4         self.linear = torch.nn.Linear(
5             hidden_size, hidden_size)
6
7     def forward(self, graph_pim, in_dense):
8         # Execute Aggregation in PIM
9         dense_parts = col_split(in_dense)
10        out_dense = gyn.pim_run_aggr(graph_pim,
11                                    dense_parts)
12        # Execute Combination in Host
13        out = self.linear(out_dense)
14        return out
15
16 # Allocate PIM Devices
17 gyn.pim_init_devices(num_pim_devices,
18                     groups_per_device)
19 data = load_dataset()
20 graph_parts = gyn.graph_split(data.graph)
21 # Load graph in PIM devices
22 graph_pim = gyn.load_csr_graph_pim(graph_parts)
23 # Create GNN model
24 model = torch.nn.Sequential([
25     Linear(in_channels, hidden_size),
26     GCNConv(hidden_size),
27     GCNConv(hidden_size),
28     GCNConv(hidden_size),
29     Linear(hidden_size, out_channels) ])
30 model.forward(graph_pim, data.features)

```

Fig. 8: GCN execution with PyGim API.

PyGim interface to run GCN inference. Programmers need to (i) allocate PIM devices, a PIM executable file is loaded into the instruction memory of PIM cores (line 17), (ii) load graph data into PIM-enabled memory (line 22), (iii) create a GNN model (lines 24-29), and (iv) run GNN inference by configuring aggregation and combination to be executed on the PIM (line 10) and Host system (line 13), respectively. The allocated PIM resources are released, when the program exits. Note that PyGim’s PIM aggregation can be also easily integrated to other ML frameworks, such as TensorFlow [1], Keras [19], MXNet [5] and Caffe [27].

IV. EVALUATION

A. Methodology

System. We evaluate PyGim on the UPMEM PIM architecture. The system consists of a Host CPU (Intel Xeon with 32 threads at 2.10 GHz), standard main memory (128 GB), and 16 PIM DIMMs of 2 ranks (124.5 GB and 1992 PIM cores at 350 MHz), each rank has 64 cores. However, there are 56 faulty cores in our evaluated system. They cannot be used and do not affect the correctness of our results, but take away from the system’s full computational power.

Models and Datasets. We evaluate GCN [29], GIN [58] and SAGE [22] models. We present detailed evaluations with 32-bit integer (**int32**) data type, since it has the same byte-width with 32-bit float (**fp32**), its arithmetic operations are more effectively supported in UPMEM PIM hardware, and provides high accuracy (having int32 for both computation and memory representation results to less than 1% accuracy drop in all models and datasets over fp32 using the quantization scheme of Ctranslate2 [7]). Quantization [7], [37], [63] is orthogonal to our optimizations, and we expect that either future PIM

Matrix Name	Rows	NNZ	Min NNZ	Max NNZ	Avg NNZ	Std NNZ
raefsky4	19779	1328611	18	177	67.17	15.96
wing_nodal	10937	150976	5	28	13.80	2.86
Dubcova2	65025	1030225	4	25	15.84	5.76
mosfet2	46994	1499460	4	162	31.91	11.71
poisson3Db	85623	2374949	6	145	27.74	14.71
smt	25710	3753184	52	414	145.98	47.52
av41092	41092	1683902	2	2135	40.98	167.04
Zd_Jac6	22835	1711983	1	1050	74.97	175.48
mycielskian15	24575	11111110	14	12287	452.13	664.17

TABLE I: Sparse matrix dataset used for one PIM core and one PIM cluster analysis.

Graph Name	Vertices	EDGs	Min EDG	Max EDG	Avg EDG	Std EDG
ogbn-proteins	132534	79122504	1	7750	597.00	621.48
Reddit	232965	114615892	1	21657	492.00	799.82
AmazonProducts	403598	156149176	1	53864	386.89	1140.91

TABLE II: Real-world graph datasets used for our large-scale experiments, when using multiple PIM DIMMs.

systems (e.g., HBM-PIM) will provide native floating-point arithmetic support or optimized quantization schemes will provide high accuracy with fixed-precision data types. We evaluate real-world sparse matrices from the Sparse Matrix Suite Collection [11], when using one PIM core and one PIM cluster. Table I presents the characteristics of these matrices, i.e., the number of rows, the number of non-zero elements (NNZs), the minimum number (min) of non-zero elements among rows, the maximum number (max) of non-zero elements among rows, the average number (avg) of non-zero elements among rows and standard deviation (std) of non-zero elements among rows. We present large-scale experiments (using multiple PIM DIMMs and devices, as well as to evaluate CPU and PIM schemes in aggregation operator and end-to-end GNN inference) with three real-world graph datasets: ogbn-proteins [52], Reddit [22] and AmazonProducts [62]. The original AmazonProducts dataset is too large to fit in a single machine, thus we split the dataset using cluster partition [6], and evaluate the largest subgraph in our experiments. Table II presents the characteristics of these real-world graph datasets, i.e., the number of vertices, the number of edges (EDGs), the minimum number (min) of edges among vertices, the maximum number (max) of edges among vertices, the average number (avg) of edges among vertices and standard deviation (std) of edges among vertices. **Comparison Points.** Combination runs on Host CPU using PyTorch. In aggregation, we compare PyGim with three schemes, the state-of-the-art matmul operator from pytorch_sparse library [15] running at 32-thread Intel Xeon CPU server (CPU), and two SpMV-based schemes running on PIM system. SparseP [17] proposes SpMV kernels for PIM systems, and shows that their optimized SpMV COO.nnz-If kernel performs best, when using ~ 2 PIM devices. We integrate this kernel in our backend and run aggregation as an SpMV execution: for each column of the feature matrix, we execute one SpMV kernel using one PIM device (SP1) or two PIM devices (SP2), and parallelize multiple SpMVs for multiple columns of feature matrix using multiple PIM devices.

B. Within PIM Core Analysis

We evaluate SpMM for int32 and fp32 with multiple threads of a PIM core. Fig. 9 presents scalability of CSR when

balancing the vertices (RV) or edges at vertex granularity (RE) across threads, and COO when balancing the edges at vertex granularity (CE) or via near-perfect edge balance using coarse-grained locking (CP-cg) or lock-free (CP-lf).

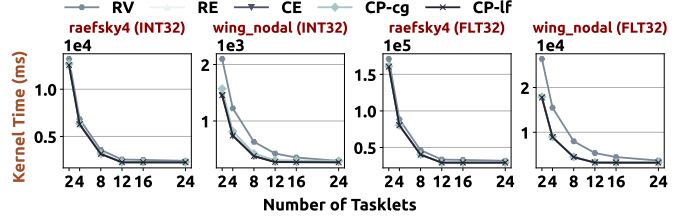


Fig. 9: Scalability of all schemes within a PIM core for the int32 (left) and fp32 (right) data types as the number of threads increases.

We draw three findings. First, all schemes scale up to 16 threads, because the PIM core pipeline is fully utilized: instructions executed in processor incur higher latency costs than memory accesses, thus the execution becomes *compute-bound*. In wing_nodal with 16 threads, only one thread process many more edges than the rest, thus RV slightly scales to 24 threads (by 0.09%), because it exhibits better compute balance across threads. Second, int32 data type provides at least one order of magnitude better performance than fp32. The UPMEM PIM core does not support in hardware floating-point operations: they are software emulated using integer arithmetic units. Third, RV provides worse performance than other schemes, since balancing the vertices across threads incurs high edge (non-zero element) imbalance, thus causing high disparity in the number of computations performed across threads.

Recommendation 1: Programmers need to minimize the amount of computations, when programming PIM cores.

Recommendation 2: Programmers can leverage quantization in ML models, if PIM cores have limited precision and arithmetic operation support in hardware.

Recommendation 3: Engineers need to enable parallelization schemes with high compute balance across threads.

C. Within PIM Cluster Analysis

Fig. 10 evaluates SpMM in one PIM cluster of 64 cores with int32 data type for CSR, when balancing the vertices (RV) or edges at vertex granularity (RE) across PIM cores, and for COO when balancing the edges at vertex granularity (CE) or via near-perfect edge balance (CP). Within each PIM core, we employ 16 threads with edge-balance across threads in CSR and near-perfect edge balance across threads (lock-free synchronization) in COO. We present the breakdown steps of Fig. 4, and sort matrices with increasing irregularity, i.e., standard deviation of non-zero elements among rows.

We draw three findings. First, the vertex-balance scheme (RV) incurs higher kernel time than edge-balance schemes

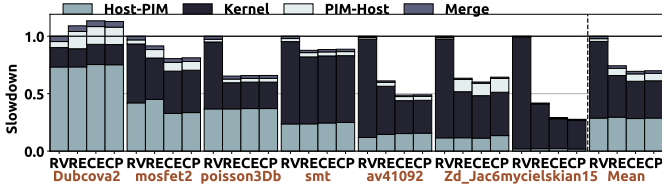


Fig. 10: Performance comparison of parallelization schemes using one PIM cluster of 64 PIM cores and various sparse matrices.

(RE, CE, CP) by $1.96\times$, because the latter provide high compute balance, i.e., similar number of edges (non-zeros) are processed across cores. Second, edge-balance schemes incur higher PIM-Host costs over vertex-balance by $2.63\times$. In UPMEM PIM, PIM-Host transfers can be performed in parallel across multiple cores if the transfer sizes from all DRAM banks are the *same*. To leverage parallel transfers, we perform padding with empty bytes (zeros) at the granularity of a PIM device, when transferring data from/to Host. Edge-balance schemes have high disparity in the number of vertices assigned to PIM cores, i.e., PIM cores produce different amount of partial results for the output matrix, thus they suffer from high amount of zero padding in PIM-Host transfers. Therefore, if a single parallelization scheme (e.g., only vertex- or edge-parallelism) is used across all available PIM cores in the system, performance would be sub-optimal, since it would cause either high kernel or high data transfer time. This key observation enhances the benefits of our proposed HP approach, that trades off computation and data transfer costs in PIM executions. Third, most matrices have a power-law distribution [53], only a few vertices have a very large number of neighbors (edges), thus edge-balance schemes provide best end-to-end performance by significantly improving kernel time. However, Dubcova2 is a relatively regular matrix, thus the vertex-balance provides enough compute balance across PIM cores, achieving $1.11\times$ better total performance than edge-balance schemes.

Recommendation 4: Software engineers can provide intelligent heuristics and algorithms that adapt their optimizations to the particular characteristics of the given input to provide high system performance in PIM executions.

Recommendation 5: Since commodity DRAM has multiple hierarchy levels (e.g., DIMM-, rank/layer-, bank group-, bank-level), each level has different characteristics in circuitry design, PIM architects can enable different hardware optimizations at each level of hierarchy. Then, system and software engineers can design different optimization techniques (e.g., different parallelization or transfer schemes) for *each* different level to enable high performance in PIM kernels via hardware, system and software co-design.

D. Across PIM Cluster Analysis

We evaluate SpMM using multiple PIM clusters and within cluster we select edge-balance schemes to minimize kernel

time. Fig. 11 presents the performance using real-world graphs, 128 hidden size, 32 PIM devices, and a *fixed* number of 1992 PIM cores while varying the parallelization scheme used: each triple of values shows the number of sparse partitions, the number of dense partitions and the number of PIM clusters per PIM device, respectively. We show breakdown steps of Fig. 4, and the stacked bar “Other” corresponds to the time needed to partition the dense matrix.

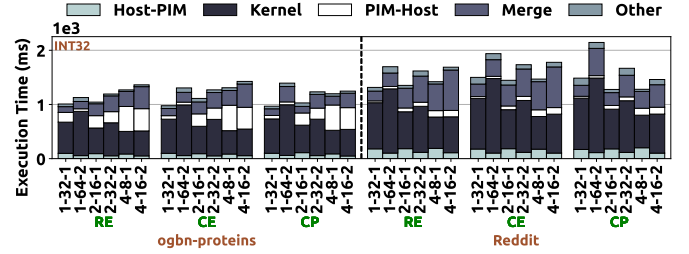


Fig. 11: Performance of edge-balance schemes, using various sparse partitions, dense partitions, and PIM clusters per device.

We note four key points. First, having 2 PIM clusters per device with ~ 28 cores per cluster increases the kernel time by $1.30\times$ on average over having 1 cluster per device of ~ 56 cores. Using a smaller number of cores per cluster results in higher compute costs, since *each* PIM core processes a larger number of edges (non-zeros), thus executing many more computations. Thus, creating PIM clusters of ~ 56 cores provides sufficient compute balance. Second, creating a larger number of sparse partitions (e.g., 4 or larger) increases PIM-Host transfer and merge overheads, since the amount of zero padding in PIM-Host transfer increases and PIM clusters create more partial results for the output matrix that are merged by Host. Third, for the same partitioning and clustering configuration, edge-balance schemes achieve similar performance, since they provide similar load balance across PIM cores. Fourth, we identify two patterns: in ogbn-proteins, best performance is achieved using CP with 1 sparse partition, while in Reddit using CP with 2 sparse partitions ($1.11\times$ better over having 1 sparse partition). In ogbn-proteins, there is a high disparity in the number of vertices assigned to PIM cores, thus a large amount of zero padding is needed in PIM-Host transfers. When increasing the sparse partitions from 1 to 2, the vertex disparity and amount of zero padding increases, thus achieving worse performance. Overall, best performance is achieved when using ~ 56 cores per PIM cluster (to minimize kernel time), and creating 1 or 2 sparse partitions (to minimize PIM-Host and merge overheads).

Recommendation 6: Programmers need to design algorithms that trade off compute time with data transfer costs to/from PIM-enabled memory.

Recommendation 7: Designers should optimize the gather collective for data transfers from PIM-enabled memory to Host, i.e., minimizing the amount of zero padding needed.

E. Scalability of PyGim Implementations

Fig. 12 presents the SpMM scalability of edge-balance schemes of PyGim, i.e., RE, CE and CP, using int32 data type. In these experiments, we have 1 sparse partition, 128 hidden size and 2 PIM clusters per PIM device, and we increase the number of PIM devices used: we evaluate 8, 16, and 32 PIM devices, i.e., the number of PIM cores increases from 456 up to 1992 (each PIM device has ~ 56 PIM cores).

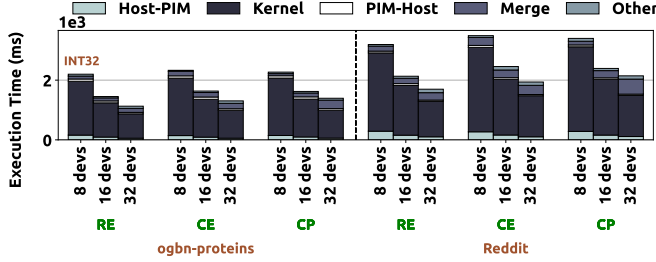


Fig. 12: Scalability of edge-balance schemes, as the number of PIM devices (correspondingly PIM cores) increases.

We find that all PyGim’s edge-balance schemes scale well. When we double the number of PIM devices used, the performance improves by $1.38\times$ on average. Thus, we conclude that PyGim is a scalable ML framework for GNN execution in real PIM systems, providing high system performance with a large number of PIM cores and PIM devices.

F. GNN Aggregation Performance

Fig. 13 compares the performance of CPU and PIM schemes (See Section IV-A) in one aggregation operator using real-world graph datasets and common hidden sizes in dense matrix (x-axis). In PIM executions, we use 32 PIM devices. In PyGim, we evaluate RE and CP schemes with 1 PIM cluster per device (~ 56 cores per cluster), and 1 and 2 sparse partitions, i.e., RE1/CP1 and RE2/CP2 schemes, respectively, resulting in 32 and 16 dense partitions, respectively.

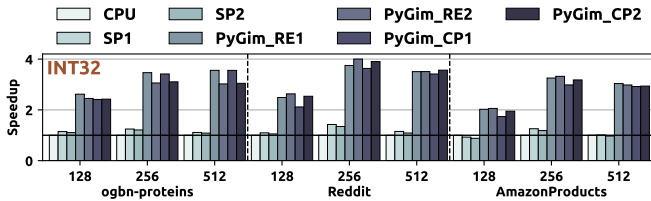


Fig. 13: Performance of CPU and PIM schemes in one aggregation, using various graphs and hidden sizes in dense matrix.

We draw three findings. First, SP1 and SP2 achieve small speedups over CPU (on average $1.14\times$), since they are optimized SpMV implementations. Instead, aggregation by its nature performs SpMM, thus PyGim schemes provide significant performance speedups, on average $3.07\times$ and up to $4.00\times$ over CPU. Second, if the hidden size is larger, PyGim provides higher speedups than that of small hidden size. For instance, PyGim outperforms CPU by $2.37\times$ and $3.45\times$ for 128 and 256 hidden size, respectively. When hidden size is

larger, the execution results in larger amount of data movement between memory and processors (exhibits lower arithmetic intensity), thus PIM systems can provide larger benefits thanks to their immense memory bandwidth available. Third, the best-performing PyGim scheme varies across datasets due to different connection characteristics between vertices. With 256 hidden size, the best-performing PyGim execution has 1 (RE1 and CP1) and 2 sparse partitions (RE2 and CP2) in ogbn-proteins and Reddit, respectively. This finding strengthens Recommendation 5: selection methods are needed to tune the parallelization scheme based on the characteristics of each particular input given. In this work, we leave for future work the exploration of tuning methods for the sparse/dense partitions in PyGim’s kernels. Overall, we conclude that PyGim provides significant performance benefits in aggregation for various widely-used graph datasets and hidden sizes in GNN inference.

Recommendation 8: Engineers can allocate multiple PIM-enabled memory modules based on the workload’s memory bandwidth needs, e.g., when using a larger hidden size, GNN aggregation has larger memory bandwidth needs, thus a larger number of PIM memory modules can be used.

G. End-to-End GNN Performance

Fig. 14, 15 and 16 evaluate CPU and PIM schemes in end-to-end GNN inference for int32, int16 and fp32 datatypes, respectively. Using various graph datasets, we evaluate 3 different GNN models, each model has 3 layers of 256 hidden size. In PIM executions, we use 32 PIM devices, having in total 1992 cores, and in PyGim RE and CP schemes we select the best-performing end-to-end execution throughput.

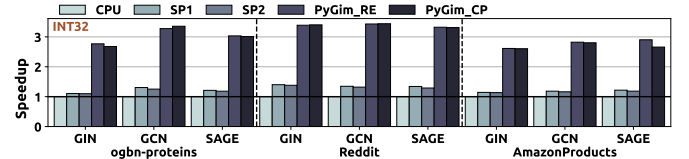


Fig. 14: Performance of CPU and PIM schemes in the end-to-end GNN inference, using various graph datasets and GNN models.

PyGim RE and CP schemes provide significant performance speedups over both their CPU counterpart and prior state-of-the-art PIM schemes (SP1 and SP2) by $3.04\times$ (up to $3.44\times$) and $2.46\times$ (up to $2.68\times$), respectively. PIM GNN execution achieves low performance with fp32 values, since their arithmetic operations are software emulated in the UPMEM PIM hardware. However, ML-oriented PIM systems are expected to be in the market soon, and will hopefully have native support for high precision data types. Instead, Fig. 15 evaluates int16 values (arithmetic operations are natively supported by PIM hardware) and shows that PyGim significantly outperforms its CPU counterpart by on average $4.23\times$ and up to $4.94\times$. When arithmetic operations are natively supported by the PIM hardware, as it happens for int16 data type in UPMEM PIM system, PIM GNN execution provides

significant performance benefits by exploiting the immense memory bandwidth available in PIM systems. Finally, we find that when using fp32 values, PIM GNN execution achieves low performance, being worse than that of CPU by on average 39.1%. This is because UPMEM PIM hardware does not support floating-point operations, which are software emulated, thus they incur high performance overheads. However, we expect that ML-oriented PIM systems will be available in the market the next few years, and will hopefully support in hardware high precision data types.

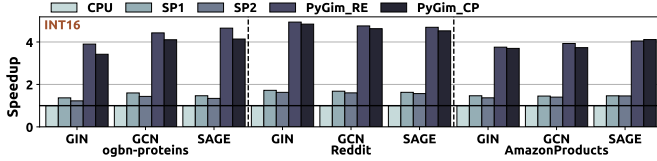


Fig. 15: Performance of CPU and PIM schemes in the end-to-end GNN inference, using various graph datasets and GNN models for int16 data type.

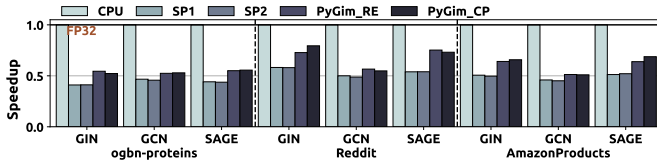


Fig. 16: Performance of CPU and PIM schemes in the end-to-end GNN inference, using various graph datasets and GNN models for fp32 data type.

H. Comparison with GPU Systems

We compare the aggregation on the UPMEM PIM system to an Intel Xeon CPU and an NVIDIA RTX3090 GPU (using matmul from pytorch_sparse), the characteristics of which are shown in Table III. For Intel Xeon CPU and NVIDIA GPU systems, we report the characteristics provided by the manufacturers. For UPMEM PIM, we report the frequency and memory capacity provided by the manufacturer. We estimate the total bandwidth as $Total_PIM_Cores * PIM_Core_Bandwidth$, where the $PIM_Core_Bandwidth$ is 700 MB/s, as measured by prior work [20], [21], and calculate the peak performance by porting and executing the peakperf [44] microbenchmark to UPMEM PIM API for int32 and fp32 data types. The source code of the microbenchmark will be open-sourced. Table IV shows the performance of int32 and fp32 aggregation using Reddit and 256 hidden size. We present an average aggregation execution time and the hardware utilization achieved in each system, which is defined as the number of operations performed divided by the execution time, and normalized as a percentage of the theoretical peak performance of the system. We calculate the number of operations performed in aggregation as $edges \times hidden_size$, which is the theoretical arithmetic operations of SpMM.

System	INT32 Exec. Time (s)	FP32 Exec. Time (s)	INT32 GOPS	FP32 GFLOPS	INT32 Hard. Utilization	FP32 Hard. Utilization
Intel Xeon 4215	7.30s	7.10s	8.04	8.26	0.63%	0.32%
UPMEM PIM	1.87s	12.74s	31.3	4.61	27.01%	18.54%
RTX3090	0.37s	0.11s	158.33	553.94	0.44%	1.56%

TABLE IV: Aggregation performance achieved in different systems.

System	Total Cores	Freq.	INT32 Peak Performance	FP32 Peak Performance	Memory Capacity	Total Bandwidth
Intel Xeon 4215	2x8 x86 cores	2.5 GHz	0.64 TOPS	1.28 TFLOPS	128 GB	23.1 GB/s
UPMEM PIM	1992 PIM cores	350 MHz	115.93 GOPS	24.85 GFLOPS	124.5 GB	1.39 TB/s
RTX3090	10496 CUDA cores	1.40 GHz	17.79 TOPS	35.58 TFLOPS	24 GB	936.2 GB/s

TABLE III: Information of the evaluated CPU, PIM and GPU systems.

GPU performs best in absolute execution time, since it has high compute throughput, $154\times$ and $1431\times$ higher than that of PIM system for int32 and fp32, respectively (Table III). GPUs were commercialized a few decades ago, and hardware architects have spent large budgets to optimize them. Instead, UPMEM PIM was released ~ 1 year ago and is still maturing: cores are expected to run at a higher frequency in the near future (500MHz instead of 350MHz) [12]. However, PyGim aggregation achieves the largest resource utilization, being $61.3\times$ and $11.8\times$ larger than that of GPU for int32 and fp32, respectively. GPU execution is bottlenecked by memory bandwidth, while PyGim’s software kernels highly exploit the compute capabilities of the underlying PIM hardware. Large resource utilization is highly desirable, since it improves the cost of ownership. Thus, we conclude that PIM is a very cost-effective solution.

V. RELATED WORK

To our knowledge, our work is the first to design an ML framework for GNN execution on PIM systems, propose hardware-efficient GNN aggregation tailored for such systems, and extensively characterize the GNN execution on the first real-world PIM system. We discuss prior work.

PIM-based GNN Accelerators. A few prior works [55], [61], [65] design PIM-based accelerators for GNNs. They place dedicated PIM units at the buffer device of ranks of memory modules, and propose DDR commands sent by CPU cores to PIM units via memory bus to control their execution. These works provide hardware designs for GNNs, use custom simulators for their evaluations and propose near-rank PIM architectures. Instead, our work provides system- and software-level optimization techniques, uses a real PIM system for evaluation, and targets near-bank PIM systems, which provide larger memory bandwidth than near-rank PIM architectures [33] and are already available in the market.

Computational Kernels for PIM Systems. Prior works [10], [13], [17], [20], [21], [26], [35] design software optimization techniques for sparse and dense linear algebra, graph processing, databases, bioinformatics, and image processing kernels tailored for PIM systems. The closest work to ours is SparseP [17], which proposes an efficient SpMV library for PIM systems. We integrate the best-performing SparseP kernel in our framework and run the aggregation step as multiple SpMV kernels. We quantitatively compare PyGim with the SparseP kernels and show that PyGim provides higher performance benefits.

GNNs and SpMM in Commodity Systems. Prior works optimize GNNs and SpMM on CPUs [2], [18], [23], [30], [60] and GPUs [9], [16], [24], [36], [42], [59] by leveraging the shared memory model of such systems and deep cache hierarchies (on-chip caches). However, their optimizations cannot be applied in PIM systems, that have a distributed memory model and shallow cache hierarchy. Prior works [3], [28], [31], [38], [39], [48], [56], [64] optimize GNNs and SpMM on distributed CPU-GPU, multi-CPU/multi-GPU systems by minimizing the communication among cores and overlapping computation with communication. Real PIM systems are fundamentally different, since typically there is no direct communication among PIM cores. Thus, well-tuned GNN and SpMM kernels for distributed processor-centric systems either cannot be directly applied in PIM systems, or having the Host to enable fine-grained inter-PIM-core communication would cause high performance overheads.

VI. CONCLUSION

We present PyGim, the first ML framework that accelerates GNNs in PIM systems, and we conduct the first characterization study of GNN inference on a real-world PIM system. We provide a hybrid GNN execution on processor-centric and memory-centric computing systems and propose intelligent parallelization techniques tailored for near-bank PIM systems to efficiently execute GNN aggregation. PyGim achieves $3.07\times$ and $3.04\times$ speedup over state-of-the-art CPU baseline in aggregation and end-to-end performance, respectively. We hope that our parallelization strategies for GNNs, in-depth PIM analysis, and open-source framework will enable further research on accelerating GNNs and other sparse ML models in memory-centric computing systems.

VII. ACKNOWLEDGEMENTS

We thank Andreas Moshovos and Bojian Zheng for their feedback and help on technical aspects of this work.

REFERENCES

- [1] M. Abadi, A. Agarwal, P. Barham, E. Brevdo, Z. Chen, C. Citro, G. S. Corrado, A. Davis, J. Dean, M. Devin *et al.*, “Tensorflow: Large-scale machine learning on heterogeneous distributed systems,” *arXiv preprint arXiv:1603.04467*, 2016.
- [2] K. Akbudak and C. Aykanat, “Exploiting locality in sparse matrix-matrix multiplication on many-core architectures,” *IEEE Transactions on Parallel and Distributed Systems*, vol. 28, no. 8, pp. 2258–2271, 2017.
- [3] V. Bharadwaj, A. Buluc, and J. Demmel, “Distributed-memory sparse kernels for machine learning,” in *2022 IEEE International Parallel and Distributed Processing Symposium (IPDPS)*, 2022.
- [4] Å. Björck, “Numerical Methods for Least Squares Problems,” in *SIAM*, 1996.
- [5] T. Chen, M. Li, Y. Li, M. Lin, N. Wang, M. Wang, T. Xiao, B. Xu, C. Zhang, and Z. Zhang, “Mxnet: A flexible and efficient machine learning library for heterogeneous distributed systems,” *arXiv preprint arXiv:1512.01274*, 2015.
- [6] W.-L. Chiang, X. Liu, S. Si, Y. Li, S. Bengio, and C.-J. Hsieh, “Clustergen: An efficient algorithm for training deep and large graph convolutional networks,” in *Proceedings of the 25th ACM SIGKDD international conference on knowledge discovery & data mining*, 2019, pp. 257–266.
- [7] Ctranslate2, “Ctranslate2,” 2023. [Online]. Available: <https://github.com/OpenNMT/CTranslate2>
- [8] L. Dagum and R. Menon, “OpenMP: An Industry-Standard API for Shared-Memory Programming,” in *IEEE Comput. Sci. Eng.*, 1998.
- [9] S. Dalton, L. Olson, and N. Bell, “Optimizing sparse matrix—matrix multiplication for the gpu,” *ACM Trans. Math. Softw.*, 2015.
- [10] P. Das, P. R. Sutradhar, M. Indovina, S. M. P. Dinakarrao, and A. Ganguly, “Implementation and evaluation of deep neural networks in commercially available processing in memory hardware,” in *2022 IEEE 35th International System-on-Chip Conference (SOCC)*, 2022, pp. 1–6.
- [11] T. A. Davis and Y. Hu, “The University of Florida Sparse Matrix Collection,” in *TOMS*, 2011.
- [12] F. Devaux, “The True Processing In Memory Accelerator,” in *Hot Chips*, 2019.
- [13] S. Diab, A. Nassereldine, M. Alser, J. Gómez Luna, O. Mutlu, and I. El Hajj, “A framework for high-throughput sequence alignment using real processing-in-memory systems,” *Bioinformatics*, vol. 39, no. 5, 2023.
- [14] W. Fan, Y. Ma, Q. Li, Y. He, E. Zhao, J. Tang, and D. Yin, “Graph neural networks for social recommendation,” in *The world wide web conference*, 2019, pp. 417–426.
- [15] M. Fey and J. E. Lenssen, “Fast graph representation learning with PyTorch Geometric,” in *ICLR Workshop on Representation Learning on Graphs and Manifolds*, 2019.
- [16] T. Gale, M. Zaharia, C. Young, and E. Elsen, “Sparse gpu kernels for deep learning,” in *SC20: International Conference for High Performance Computing, Networking, Storage and Analysis*. IEEE, 2020, pp. 1–14.
- [17] C. Giannoula, I. Fernandez, J. G. Luna, N. Koziris, G. Goumas, and O. Mutlu, “Sparsep: Towards efficient sparse matrix vector multiplication on real processing-in-memory architectures,” *Proceedings of the ACM on Measurement and Analysis of Computing Systems*, vol. 6, no. 1, pp. 1–49, 2022.
- [18] Z. Gong, H. Ji, Y. Yao, C. W. Fletcher, C. J. Hughes, and J. Torrellas, “Graphite: Optimizing graph neural networks on cpus through cooperative software-hardware techniques,” in *Proceedings of the 49th Annual International Symposium on Computer Architecture*, 2022.
- [19] A. Gulli and S. Pal, *Deep learning with Keras*. Packt Publishing Ltd, 2017.
- [20] J. Gómez-Luna, Y. Guo, S. Brocard, J. Legriel, R. Cimadomo, G. F. Oliveira, G. Singh, and O. Mutlu, “Evaluating machine learning workloads on memory-centric computing systems,” in *2023 IEEE International Symposium on Performance Analysis of Systems and Software (ISPASS)*, 2023, pp. 35–49.
- [21] J. Gómez-Luna, I. E. Hajj, I. Fernandez, C. Giannoula, G. F. Oliveira, and O. Mutlu, “Benchmarking a new paradigm: Experimental analysis and characterization of a real processing-in-memory system,” *IEEE Access*, vol. 10, pp. 52 565–52 608, 2022.
- [22] W. Hamilton, Z. Ying, and J. Leskovec, “Inductive representation learning on large graphs,” *Advances in neural information processing systems*, vol. 30, 2017.
- [23] C. Hong, A. Sukumaran-Rajam, I. Nisa, K. Singh, and P. Sadayappan, “Adaptive sparse tiling for sparse matrix multiplication,” in *Proceedings of the 24th Symposium on Principles and Practice of Parallel Programming*, 2019.
- [24] K. Huang, J. Zhai, Z. Zheng, Y. Yi, and X. Shen, “Understanding and bridging the gaps in current gnn performance optimizations,” in *Proceedings of the 26th ACM SIGPLAN Symposium on Principles and Practice of Parallel Programming*, 2021.
- [25] E. Im and K. A. Yelick, “Optimizing Sparse Matrix Vector Multiplication on SMP,” in *PPSC*, 1999.
- [26] M. Item, G. F. Oliveira, J. Gómez-Luna, M. Sadrosadati, Y. Guo, and O. Mutlu, “Transpimlib: Efficient transcendental functions for processing-in-memory systems,” in *2023 IEEE International Symposium on Performance Analysis of Systems and Software (ISPASS)*, 2023, pp. 235–247.
- [27] Y. Jia, E. Shelhamer, J. Donahue, S. Karayev, J. Long, R. Girshick, S. Guadarrama, and T. Darrell, “Caffe: Convolutional architecture for fast feature embedding,” in *Proceedings of the 22nd ACM international conference on Multimedia*, 2014, pp. 675–678.
- [28] Z. Jia, S. Lin, M. Gao, M. A. Zaharia, and A. Aiken, “Improving the accuracy, scalability, and performance of graph neural networks with roc,” in *Conference on Machine Learning and Systems*, 2020.
- [29] T. N. Kipf and M. Welling, “Semi-supervised classification with graph convolutional networks,” *arXiv preprint arXiv:1609.02907*, 2016.
- [30] F. Kjolstad, S. Kamil, S. Chou, D. Lugato, and S. Amarasinghe, “The tensor algebra compiler,” *Proc. ACM Program. Lang.*, 2017.
- [31] P. Koanantakool, A. Azad, A. Buluç, D. Morozov, S.-Y. Oh, L. Oliker, and K. Yelick, “Communication-avoiding parallel sparse-dense matrix-matrix

- multiplication,” in *2016 IEEE International Parallel and Distributed Processing Symposium (IPDPS)*, 2016, pp. 842–853.
- [32] D. Langr and P. Tvrdík, “Evaluation Criteria for Sparse Matrix Storage Formats,” in *TPDS*, 2016.
- [33] S. Lee, K. Kim, S. Oh, J. Park, G. Hong, D. Ka, K. Hwang, J. Park, K. Kang, J. Kim *et al.*, “A l1nm 1.25 v 8gb, 16gb/s/pin gddr6-based accelerator-in-memory supporting 1tflops mac operation and various activation functions for deep-learning applications,” in *2022 IEEE International Solid-State Circuits Conference (ISSCC)*, vol. 65. IEEE, 2022, pp. 1–3.
- [34] S. Lee, S.-h. Kang, J. Lee, H. Kim, E. Lee, S. Seo, H. Yoon, S. Lee, K. Lim, H. Shin, J. Kim, O. Seongil, A. Iyer, D. Wang, K. Sohn, and N. S. Kim, “Hardware architecture and software stack for pim based on commercial dram technology : Industrial product,” in *2021 ACM/IEEE 48th Annual International Symposium on Computer Architecture (ISCA)*, 2021, pp. 43–56.
- [35] C. Lim, S. Lee, J. Choi, J. Lee, S. Park, H. Kim, J. Lee, and Y. Kim, “Design and analysis of a processing-in-dimm join algorithm: A case study with upmem dimms,” *Proc. ACM Manag. Data*, 2023.
- [36] W. Liu and B. Vinter, “An efficient gpu general sparse matrix-matrix multiplication for irregular data,” in *2014 IEEE 28th International Parallel and Distributed Processing Symposium*, 2014, pp. 370–381.
- [37] D. M. Lorocho, N. Wehn, F.-J. Pfreundt, and J. Keuper, “Tensorquant - a simulation toolbox for deep neural network quantization,” in *arXiv*, 2017.
- [38] L. Ma, Z. Yang, Y. Miao, J. Xue, M. Wu, L. Zhou, and Y. Dai, “Neugraph: Parallel deep neural network computation on large graphs,” in *Proceedings of the 2019 USENIX Conference on Usenix Annual Technical Conference*, 2019.
- [39] V. Md, S. Misra, G. Ma, R. Mohanty, E. Georganas, A. Heinecke, D. Kalamkar, N. K. Ahmed, and S. Avancha, “Distgcn: Scalable distributed training for large-scale graph neural networks,” in *Proceedings of the International Conference for High Performance Computing, Networking, Storage and Analysis*, 2021.
- [40] P. Mpakos, D. Galanopoulos, P. Anastasiadis, N. Papadopoulou, N. Koziris, and G. Goumas, “Feature-based spmv performance analysis on contemporary devices,” in *2023 IEEE International Parallel and Distributed Processing Symposium (IPDPS)*, 2023.
- [41] O. Mutlu, S. Ghose, J. Gómez-Luna, and R. Ausavarungnirun, “A Modern Primer on Processing in Memory,” in *Emerging Computing: From Devices to Systems - Looking Beyond Moore and Von Neumann*, 2021. [Online]. Available: <https://arxiv.org/pdf/2012.03112.pdf>
- [42] Y. Niu, Z. Lu, H. Ji, S. Song, Z. Jin, and W. Liu, “Tilepgemm: A tiled algorithm for parallel sparse general matrix-matrix multiplication on gpus,” in *Proceedings of the 27th ACM SIGPLAN Symposium on Principles and Practice of Parallel Programming*, 2022.
- [43] A. Paszke, S. Gross, F. Massa, A. Lerer, J. Bradbury, G. Chanan, T. Killeen, Z. Lin, N. Gimelshein, L. Antiga *et al.*, “Pytorch: An imperative style, high-performance deep learning library,” *Advances in neural information processing systems*, vol. 32, 2019.
- [44] peakperf, “peakperf,” 2021. [Online]. Available: <https://github.com/Dr-Noob/peakperf.git>
- [45] A. Pinar and M. T. Heath, “Improving Performance of Sparse Matrix-Vector Multiplication,” in *SC*, 1999.
- [46] U. W. Pooch and A. Nieder, “A Survey of Indexing Techniques for Sparse Matrices,” in *ACM Comput. Surv.*, 1973.
- [47] G. Qian, A. Abualshour, G. Li, A. Thabet, and B. Ghanem, “Pu-gcn: Point cloud upsampling using graph convolutional networks,” in *Proceedings of the IEEE/CVF Conference on Computer Vision and Pattern Recognition*, 2021, pp. 11 683–11 692.
- [48] O. Selvitopi, B. Brock, I. Nisa, A. Tripathy, K. Yelick, and A. Buluç, “Distributed-memory parallel algorithms for sparse times tall-skinny-dense matrix multiplication,” in *Proceedings of the ACM International Conference on Supercomputing*, 2021.
- [49] S. Sengupta, M. Harris, Y. Zhang, and J. D. Owens, “Scan Primitives for GPU Computing,” in *GH*, 2007.
- [50] C. Shang, J. Chen, and J. Bi, “Discrete graph structure learning for forecasting multiple time series,” in *International Conference on Learning Representations*, 2021.
- [51] J. M. Stokes, K. Yang, K. Swanson, W. Jin, A. Cubillos-Ruiz, N. M. Donghia, C. R. MacNair, S. French, L. A. Carfrae, Z. Bloom-Ackermann *et al.*, “A deep learning approach to antibiotic discovery,” *Cell*, vol. 180, no. 4, pp. 688–702, 2020.
- [52] D. Szklarczyk, A. L. Gable, D. Lyon, A. Junge, S. Wyder, J. Huerta-Cepas, M. Simonovic, N. T. Doncheva, J. H. Morris, P. Bork *et al.*, “String v11: protein–protein association networks with increased coverage, supporting functional discovery in genome-wide experimental datasets,” *Nucleic acids research*, vol. 47, no. D1, pp. D607–D613, 2019.
- [53] W. T. Tang, R. Zhao, M. Lu, Y. Liang, H. P. Huynh, X. Li, and R. S. M. Goh, “Optimizing and auto-tuning scale-free sparse matrix-vector multiplication on intel xeon phi,” in *2015 IEEE/ACM International Symposium on Code Generation and Optimization (CGO)*. IEEE, 2015, pp. 136–145.
- [54] J. Thorpe, Y. Qiao, J. Eyolfson, S. Teng, G. Hu, Z. Jia, J. Wei, K. Vora, R. Netravali, M. Kim, and G. H. Xu, “Dorylus: Affordable, scalable, and accurate GNN training with distributed CPU servers and serverless threads,” in *15th USENIX Symposium on Operating Systems Design and Implementation (OSDI 21)*, 2021.
- [55] T. Tian, X. Wang, L. Zhao, W. Wu, X. Zhang, F. Lu, T. Wang, and X. Jin, “G-nmp: Accelerating graph neural networks with dimm-based near-memory processing,” *Journal of Systems Architecture*, vol. 129, p. 102602, 2022.
- [56] A. Tripathy, K. Yelick, and A. Buluç, “Reducing communication in graph neural network training,” in *Proceedings of the International Conference for High Performance Computing, Networking, Storage and Analysis*, 2020.
- [57] S. Wu, Y. Tang, Y. Zhu, L. Wang, X. Xie, and T. Tan, “Session-based recommendation with graph neural networks,” in *Proceedings of the AAAI conference on artificial intelligence*, vol. 33, no. 01, 2019, pp. 346–353.
- [58] K. Xu, W. Hu, J. Leskovec, and S. Jegelka, “How powerful are graph neural networks?” *arXiv preprint arXiv:1810.00826*, 2018.
- [59] C. Yang, A. Buluç, and J. D. Owens, “Design principles for sparse matrix multiplication on the gpu,” in *European Conference on Parallel Processing*. Springer, 2018, pp. 672–687.
- [60] S. Yesil, J. E. Moreira, and J. Torrellas, “Dense dynamic blocks: optimizing spmm for processors with vector and matrix units using machine learning techniques,” in *Proceedings of the 36th ACM International Conference on Supercomputing*, 2022, pp. 1–14.
- [61] S. Yun, H. Nam, J. Park, B. Kim, J. H. Ahn, and E. Lee, “Grande: Efficient near-data processing architecture for graph neural networks,” *IEEE Transactions on Computers*, 2023.
- [62] H. Zeng, H. Zhou, A. Srivastava, R. Kannan, and V. Prasanna, “Graph-saint: Graph sampling based inductive learning method,” *arXiv preprint arXiv:1907.04931*, 2019.
- [63] T. Zhang, Z. Lin, G. Yang, and C. D. Sa, “Qpytorch: A low-precision arithmetic simulation framework,” in *arXiv*, 2019. [Online]. Available: <https://github.com/Tiiiger/QPyTorch/tree/master>
- [64] D. Zheng, C. Ma, M. Wang, J. Zhou, Q. Su, X. Song, Q. Gan, Z. Zhang, and G. Karypis, “Distdgl: Distributed graph neural network training for billion-scale graphs,” in *2020 IEEE/ACM 10th Workshop on Irregular Applications: Architectures and Algorithms (IA3)*, 2020.
- [65] Z. Zhou, C. Li, X. Wei, X. Wang, and G. Sun, “Gnnear: Accelerating full-batch training of graph neural networks with near-memory processing,” in *Proceedings of the International Conference on Parallel Architectures and Compilation Techniques*, 2022, pp. 54–68.